Journal of Nuclear Materials 383 (2009) 231–236

Contents lists available at ScienceDirect

Journal of Nuclear Materials

journal homepage: www.elsevier.com/locate/jnucmat

Radiation chemical synthesis and characterization of UO_2 nanoparticles

Olivia Roth *, Hanna Hasselberg, Mats Jonsson

KTH Chemical Science and Engineering, Nuclear Chemistry, Royal Institute of Technology, Teknikringen 36, SE-100 44 Stockholm, Sweden

ARTICLE INFO

Article history:
Received 30 June 2008
Accepted 16 September 2008

ABSTRACT

In a deep repository for spent nuclear fuel, U(VI)(aq) released upon dissolution of the fuel matrix could, in reducing parts of the system, be converted to U(IV) species which might coalesce and form nanometer-sized UO_2 particles. This type of particles is expected to have different properties compared to bulk UO_2(s). Hence, their properties, in particular the capacity for oxidant consumption, must be investigated in order to assess the effects of formation of such particles in a deep repository. In this work, methods for radiation chemical synthesis of nanometer-sized UO_2 particles, by electron- and γ-irradiation of U(VI) solutions, are presented. Electron-irradiation proved to be the most efficient method, showing high conversions of U(VI) and yielding small particles with a narrow size distribution (22–35 nm). Stable colloidal suspensions were obtained at low pH and ionic strength (pH 3, I = 0.03). Furthermore, the reactivity of the produced UO_2 particles towards H_2O_2 is investigated. The U(IV) fraction in the produced particles was found to be ~20% of the total uranium content, and the results show that the UO_2 nanoparticles are significantly more reactive than micrometer-sized UO_2 when it comes to H_2O_2 consumption, the major part of the H_2O_2 being catalytically decomposed on the particle surface.

1. Introduction

The oxidative dissolution of UO_2 has been extensively studied due to its importance in the safety assessment of a future geological repository for spent nuclear fuel [1,2]. Dissolution of the UO_2 matrix, making up ~95% of the spent fuel, is expected to control the release of radionuclides in case of barrier failure [1]. In the reducing environment expected at the depth of a deep repository, the solubility of the UO_2 matrix is very low [3] and the release of radionuclides is prevented. Under oxidizing conditions the solubility of the matrix is, however, significantly increased [4].

When water comes into contact with the spent fuel, reducing and oxidizing radiolysis products will be formed. Reaction between oxidants and the UO_2 matrix will produce U(VI) on the fuel surface. The presence of complexing agents, e.g., carbonate, will lead to efficient removal of U(VI) from the surface by the formation of soluble carbonate complexes [5] and cause spreading of U(VI) and radionuclides contained by the matrix.

Under these conditions (when U(VI) is rapidly removed from the surface), the radiolytically formed reductants will be of minor importance since the surface available for reducing species will be very small. Hence, the region close to the fuel surface will be dominated by the oxidants whereas the reducing species dominate at further distance from the fuel surface. When reaching these reducing parts of the system, the dissolved U(VI) species can be converted to U(IV), which might coalesce and form nanometer-sized UO_2 particles.

This type of process (radiation chemical production of nanoparticles) is a well-known method for production of nanoparticles of semiconductors [6–8] and metal-oxides [9]. The fundamentals of this method are the reduction or, in some cases, oxidation of dissolved ionic metal/semiconductor species by radiolytically produced reducing or oxidizing agents, followed by colloid formation by coalescence. The reducing (or oxidizing) agents used in the nanoparticle production are formed by exposing the solvent to ionizing radiation. The energy deposit in the solvent causes radiolysis and the formation of a number of reactive species. Radiolysis of water produces strong reducing agents such as e^-_{aq} and H·, but also oxidizing species such as OH·. In laboratory synthesis, reducing conditions (or oxidizing when desired) are obtained by addition of scavengers – typically secondary alcohols, e.g., 2-propanol. The secondary alcohol reacts with both OH· and H· forming a strongly reducing radical according to the following reaction [10].

$$H_3C{-}CHOH{-}CH_3 + OH^{\bullet}(H^{\bullet}) \rightarrow (CH_3)_2{-}C^{\bullet}OH + H_2O(H_2) \qquad (1)$$

The reaction between the radiolytically produced reductants and metal/semiconductor ionic species produces atoms/molecules (M^0), uniformly distributed in the solution. When colliding, they dimerize (reaction (2)) and M_2 then coalesce into larger clusters. The dimerization (followed by coalescence) can also take place between atoms/molecules or clusters and unreduced ions (M^+) (reaction (3)) [10]

* Corresponding author. Tel.: +46 8 7909279; fax: +46 8 7908772.
E-mail address: oliviar@kth.se (O. Roth).

0022-3115/$ - see front matter © 2008 Elsevier B.V. All rights reserved.
doi:10.1016/j.jnucmat.2008.09.026

$$M^0 + M^0 \rightarrow M_2 \quad (2)$$

$$M^0 + M^+ \rightarrow M_2^+ \quad (3)$$

If continuous radiation (low dose rate) is used, the dimerization and coalescence occur parallel to the production and scavenging of the reducing species. Hence, the cluster growth is dominated by the later process (reaction (3)), and the reduction occurs mostly on the clusters already formed. The result is larger clusters compared to the ones formed using pulsed radiation (high dose rate), where the production and scavenging of the reducing species occur within a short time range giving rise to a large number of separate atoms/molecules, and the cluster growth is controlled by the following coalescence [10]. The final particle size is determined by the prevention of coalescence of clusters beyond certain nuclearity. This can, e.g., be controlled by using a polymeric molecule anchored to the cluster, thus preventing further coalescence through electrostatic repulsion or steric hindrance [10].

The conversion of U(VI) to U(IV) by reducing radiolysis products in organic solvents has been studied to some extent by Dzięgielewski et al. [11–14]. The production of UO_2 by homogeneous reduction of U(VI) by H_2 has also been studied [15]. In this study the composition of the solid product was confirmed by X-ray diffraction. Some evidence of the formation of UO_2 colloids from the aqueous corrosion of metallic uranium fuel (and possibly also from UO_2 fuel) has also been found by Kaminski et al. [16].

In many of the experimental investigations concerning oxidative dissolution of spent nuclear fuel, UO_2 has been used as a model substance for spent nuclear fuel when studying the mechanisms and kinetics of elementary processes involved in spent fuel dissolution [17–21]. These studies have provided information on the reactivity of bulk (micrometer-sized) UO_2 towards various oxidation agents. It is, however, reasonable to believe that the properties of UO_2 nanoparticles should be different from the bulk UO_2 used in these previous studies. This issue must be investigated in order to predict the effect of production of UO_2 nanoparticles in a future deep repository.

Compared to nanoparticles of other semiconductors and metals, e.g., silver, which has been extensively studied in the area of photographic development [22], the knowledge of UO_2 nanoparticles is still scarce. The production of UO_2 nanoparticles by laser evaporation has been studied by Salikhov and Kan [23]. Electrochemically produced UO_2 colloids have also been used in some UO_2 dissolution experiments performed by Mennecart et al. [24,25] and Grambow et al. [26].

The size dependence of the kinetic parameters for reaction between solute reactants and solid particles has been studied in different systems. Early studies of the oxidation of magnetite revealed that the grain size affected the reaction rate [27] and possibly also the mechanism of the reaction [28]. Astumian and Shelly [29] derived a relationship describing the particle size dependence of the reaction rate for reactions between solutes and suspended particles with spherical geometry (Eq. (4)). In the system studied here, the solute consists of dissolved oxidant (OX) and the suspended particles of solid metal-oxide particles (MOX).

$$\frac{d[OX]}{dt} = -\frac{2k_B T}{3\pi\eta}\frac{R_{MOX}^2}{R_{OX}R_p}\left(e^{-\frac{E_a}{RT}}\right)[OX]\frac{N_{MOX(surf)}}{V} \quad (4)$$

k_B, T and η denote the Boltzmann constant, the absolute temperature and the viscosity of the solvent, [OX] denotes the concentration of oxidant in solution, R_p denotes the radius of the suspended metal-oxide particles and R_{OX} and R_{MOX} are the molecular radii of the oxidant and the solid metal-oxide material, respectively. $N_{MOX(surf)}$ denotes the number of solid phase molecules on the particle surface being exposed to the solution of volume V. From Eq. (4) it is obvious that the pre-exponential factor decreases with increasing particle size.

It has also been suggested that, for the reaction between iron oxides and H_2O_2, not only the pre-exponential factor but also the activation energy is particle size dependent and that the dependence (deviation from bulk material) can be described by Eq. (5), originating from the Boltzmann distribution [30].

$$-\Delta E_a = k_B T \ln\frac{N_{MOX(surf)}}{N_{MOX(bulk)}} = k_B T \ln\frac{1}{R_p} \quad (5)$$

where $N_{MOX(surf)}$ and $N_{MOX(bulk)}$ denote the number of molecules on the surface and the total molecule content of the particle, respectively. Consequently, the activation energy is expected to decrease with increasing particle size.

When substituting the activation energy in Eq. (4) with the expression derived in Eq. (5) we find that the particle size (R_p) is cancelled from the equation. That is, the particle size effect on the pre-exponential factor and the activation energy cancel each other completely, hence, on the basis of these equations we can expect no effect on the rate constant for electron transfer from a change in particle size.

In practice, the second-order rate constants for heterogeneous reactions are normally determined by monitoring the concentration of solute reactant as a function of reaction time. When an excess of solid material is used, the reaction will be of pseudo-first-order, and the pseudo-first-order rate constant can be obtained from the slope when plotting the logarithm of the solute reactant concentration versus time. By repeating this procedure for a number of different solid surface areas to solution volume ratios, the second-order rate constant can be determined from the slope when plotting the pseudo-first-order rate constant as a function of surface area to solution volume ratio. Since the surface area to solution volume ratio has the unit m^{-1}, the unit for the second-order rate constant of the heterogeneous reaction is $m\ s^{-1}$.

The second-order rate constants and activation energies have previously been determined for the reaction between UO_2 powder of different size fractions and MnO_4^- in aqueous solution and the results were found to agree quite well with Eqs. (4) and (5), i.e., changing the particle size did not affect the rate constant (based on geometrically calculated particle surface) significantly, whereas the activation energy was found to increase with decreasing particle size [31]. The particles investigated in this study were, however, all of micrometer size and it has been known for long that smaller particles (nanometer range) behave differently from bulk material [32]. Around 1970, studies of reduction of copper in liquid ammonia [33] and reduction of silver in water [34] revealed apparent anomalies in the behavior of the nanoparticles. The effects were later explained by concluding that the atoms and aggregates exhibit specific thermodynamic properties different from those of the bulk material due to quantum mechanical effects [33]. The energy levels in small particles approach those of single molecules. In bulk material, the energy levels are continuously distributed, whereas in single molecules they are discrete. When decreasing the particle size, the levels of the valence band are moderately shifted to lower energies, while there is a strong shift to higher energies for the conduction band [35]. Hence, the quantum mechanical effect gives rise to a broader band gap between the valence band and the conduction band in small particles compared to the bulk material, which lead to a higher activation energy for oxidation of small particles. This is consistent with Eq. (5) and also with previous findings [31]. Nurmi et al. [36] have studied the particle size dependence of the reactivity of metallic iron particles and determined higher mass-normalized rate constants for nanometer-sized particles, compared to micrometer-sized particles. No differences could, however, be observed in the surface area-normalized

rate constants. The authors attribute this to difficulties in determination of the surface area of the nanoparticles.

In this work, a method for synthesis of nanometer-sized UO_2 particles is presented. The produced nanoparticles are characterized by measuring the particle size distribution and BET-surface and the influence of pH and ionic strength on the particle size distribution and stability of the produced colloidal suspensions are studied. Furthermore, the reactivity of the UO_2 particles towards H_2O_2 is investigated and the U(IV) content is estimated.

The possibility of formation of UO_2 nanoparticles conditions relevant to a deep repository for spent nuclear fuel is also investigated and discussed.

2. Experimental methods

The synthesis of UO_2 nanoparticles was performed by irradiation of 10 mM UO_2^{2+} (uranylnitrate) solutions containing 10% 2-propanol, total volume 20 mL. The irradiation sources used were a Co-60 γ-source (0.055 Gy/s) and a microtrone electron accelerator (6 MeV, pulse frequency 12.5 Hz, 4 μs pulse duration). The average dose rate in the electron accelerator was measured to ~24 Gy/s by Fricke dosimetry (corresponding to $\sim 10^8$ Gy/pulse). The electron-irradiations were performed in 0.5–4 min intervals. The irradiations were performed in closed glass vessels, and the solutions were purged with Ar(g) prior to the irradiations, in order to prevent oxygen influence.

In the experiments using electron-irradiation, the ionic strength and pH were varied (by addition of $NaHCO_3$, Na_2SO_4 and Na_2CO_3) in order to investigate the effects on the particle size distribution and stability of the produced colloidal suspensions.

The particle suspensions were analyzed by photon correlation spectroscopy (PCS) using a BI-90 particle sizer, Brookhaven Instruments Co., USA with wavelength 488 nm and fixed scattering angle 90°. The count rate (photon counts per second) given by the instrument is proportional to the concentration of particles, but can also be affected by the refractive index and the geometry of the particles. PCS was also used to determine the particle size distribution of the colloids. When producing the nanoparticles by Co-60 γ-irradiation the particle size was monitored as a function of irradiation.

The conversion of U(VI) was determined by filtering the suspensions and measuring the U(VI) concentration in the aqueous phase as a function of irradiation time. Three methods, all giving similar results, were used to determine the U(VI) concentration; Scintrex measurements, UV/Vis spectroscopy at 420 nm (Jasco V-350 UV/Vis Spectrophotometer) and UV/Vis spectroscopy at 653 nm using the Arsenazo(III) reagent (ε_{653} = 63 000 [36]). For the latter method, a sample of the solution was mixed with 40 μL 0.3% As(III) in ~10% acetic acid and 40 μL 1.6 M HCl and water to a total volume of 1.5 mL. Detailed information about this method is found in Refs. [37,38].

In order to measure the specific surface area of the particles the solid was precipitated by addition of NaOH. Thereafter, the solution was removed by filtration under Ar(g) pressure and the solid phase was dried in inert atmosphere. The specific surface area was measured by the BET isotherm using a Micromeritics Flowsorb II 2300 with 30% N_2 in helium.

The formation of UO_2 nanoparticles by electron-irradiation was also investigated in the absence of 2-propanol. In these experiments, 10% *tert*-butanol was used in the reaction solution in order to scavenge OH·. The H_2O_2 consumption of these particles was measured.

For the reactivity study, fresh colloidal suspensions were synthesized by electron-irradiation (10 mM UO_2^{2+}, 10% 2-propanol in 20 mL solution, as above), total irradiation time 14 min. The produced suspensions were placed in a glove box (inert atmosphere, < 0.1 ppm O_2) directly after irradiation. At the start of each reactivity experiment, the desired amount of UO_2 colloids was withdrawn from the production vessel by pipetting the corresponding suspension volume (assuming that the particles are homogeneously distributed in the solution). Several experiments were performed, with the amount of added colloidal suspension varying from 1.5 to 3.5 mL (theoretically corresponding to 4.3–10.1 mg of UO_2 powder).

The suspension was added to the reaction solution containing ~0.12 mM H_2O_2 and 10 mM $NaHCO_3$, total volume 400 mL. The reaction solution was stirred with a magnetic stirrer throughout the experiment. The H_2O_2 concentration in the solution was monitored as a function of time. I_3^- was used as an indicator for indirect analysis of the H_2O_2 concentration by UV/Vis spectroscopy at 360 nm (where I_3^- absorbs) according to the following reactions.

$$H_2O_2 + 2H^+ + 2I^- \rightarrow 2H_2O + I_2 \quad (6)$$

$$I_2 + I^- \rightarrow I_3^- \quad (7)$$

A small sample (400 μL) was taken from the reaction vessel. The sample was mixed with 100 μL 1 M KI solution, 100 μL acetate buffer (1 M HAc/NaAc, a few drops of 3% $(NH_4)_2Mo_2O_7$ (ADM) to 100 mL solution) and water to a total volume of 2 mL. Detailed information about this method can be found in Refs. [39–41].

The uncertainty in the determination of U(VI) and H_2O_2 concentrations is estimated to be <10%. The chemicals were supplied by Lancaster, Merck, Alfa, BHD and AGA and were of the purest grade available. Millipore Milli-Q filtered water was used throughout this work.

3. Results and discussion

3.1. UO_2(s) synthesis using electron accelerator

Immediately after the irradiations it could be seen, by visual inspection, that the solutions had changed from being yellow and clear to dark grey and turbid. The colloids produced at pH 3 and I = 0.03 M were analyzed with PCS. The PCS measurements of the fresh (<1 day old) powder revealed a narrow size distribution around 22–35 nm and the measured BET-surface area after precipitation was 60–70 m^2/g. Using the BET-area, assuming spherical particles, the diameter of the particles was calculated to ~9 nm, which is in good agreement with the measured size distribution. These colloidal solutions were stable, i.e., no sedimentation was observed (after ~1 month). However, the size of the particles increase with time and after ~1 month the particle size was around 50 nm, which indicates that slow aggregation occurs.

The colloidal suspensions produced at high ionic strength (I = 0.18 M), on the other hand, were not stable and the measured initial particle size was significantly higher, around 400 nm. The rationale for this is that increasing ionic strength decreases the repulsion between colloidal particles and thus facilitates aggregation. When varying the pH (3.6, 5.45, 7 and 11.4) at constant ionic strength (I = 0.18), it was found that the smallest particles (and the highest number of particles) were formed at pH 11.4. This indicates that the stability of the colloid suspension increases with increasing pH. This is reasonable since pH 11.4 is far from the pzc[1] and the particles are highly charged (high surface potential), which increases the repulsion between colloidal particles, thus preventing aggregation. The aggregation/precipitation (studied at pH 5.45 and 11.4) seems to follow first-order kinetics. The precipitate was black/dark grey.

[1] The point of zero charge (pzc) of UO_2 has been determined to pH 5–5.5 for I = 0.1 and 0.01 M [42].

The conversion of uranyl (at I = 0.03 and pH 3), determined from the measurement of U(VI) in solution after irradiation, is shown as a function of absorbed dose and irradiation time in Fig. 1. As can be seen, the conversion increases linearly with absorbed dose up to ~85%, after which the conversion rate decreases. The maximum conversion (95%) is reached at about 15 kGy. The radiation chemical yield (G-value) of reducing radicals in this system is 0.56 μmol/J [43]. Since each reducing radical transfers only one-electron, the theoretical yield of U(IV) is 0.28 μmol/J. Based on U(VI) consumption in our experiments, assuming reduction to be the only process responsible for removal of U(VI) from solution, the calculated yield of UO_2 is ~1.4 μmol/J. This is higher than the theoretical yield, indicating that the produced solid also contains uranium of higher oxidation states, as observed earlier by Dzięgielewski et al. [13]. Based on the calculated yield, only ~20% of the total uranium content in the powder consists of U(IV). Apart from U(IV), U(V) and U(VI) are probably also present in the produced solid, either co-precipitated with U(IV) or sorbed to the surface of the nanoparticles.

The conversion of uranyl in the *tert*-butanol system is shown in Fig. 1. In these systems the solvated electron (G-value 0.28 μmol/J) is the only reducing radical present and the G-value calculated based on uranyl conversion is 0.8 μmol/J. This is in good agreement with the observations in the 2-propanol system and indicates that the powder produced in the *tert*-butanol system also consists of ~20% U(IV).

3.2. UO_2(s) synthesis using Co-60 γ-irradiation

Production of nanoparticles in the Co-60 γ-source required considerably longer irradiation times compared to electron-irradiation, due to the low dose rate. The particle size increased with irradiation time and after ~7 days of irradiation it was around 80 nm, i.e., significantly larger than the particles produced by electron-irradiation. This is consistent with the relationship between dose rate and size of the produced particles discussed in Section 1.

The conversion of uranyl (at pH 3 and I = 0.03) is shown as a function of irradiation time and dose in Fig. 2. The initial production rate gives a G-value of ~0.3 μmol/J which agrees quite well with the theoretical yield (0.28 μmol/J). As can be seen in the figure the production rate is reduced and the system seems to reach steady-state after about 70 h of irradiation. The maximum conversion reached is ~65%.

The maximum conversion is significantly lower compared to the electron-irradiated system. This could perhaps be attributed to the production of H_2O_2 during irradiation. In the γ-irradiated case, a higher dose is required to reach the maximum conversion, this leads to a higher amount of H_2O_2 being produced in the system. It is possible that the limit of 65% conversion is due to a steady-state between UO_2 nanoparticle production and consumption by radiolytically produced H_2O_2.

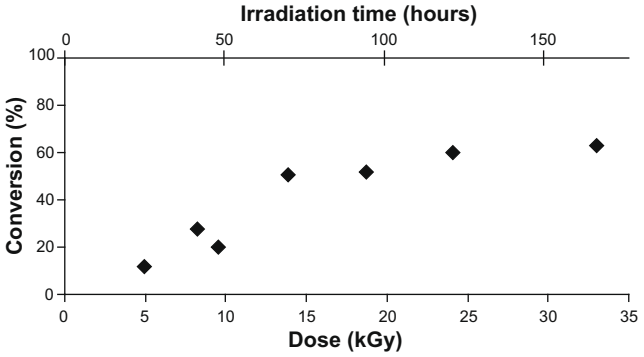

Fig. 2. Conversion of U(VI) as a function of irradiation time and absorbed dose, γ-irradiation.

3.3. Reactivity of the nano-sized UO_2(s)

When studying the reactivity in this kind of system, the goal is normally to determine the second-order rate constant. The procedure for this has been described above. A prerequisite for this type of experiments is that the reaction rate gives reasonable sampling times. Usually, this can be achieved by an appropriate choice of the amount of solid material and the solution volume (i.e., the surface area/volume ratio). Furthermore, the initial oxidant concentration must be low enough to maintain the excess of solid material, but high enough to obtain measurable changes in concentration as the reaction proceeds. In the present system, the large specific surface area of the UO_2 particles made this impossible. Only an unreasonably large reaction volume, which would have influenced the mixing of the system, would have given a measurable first-order reaction rate. Hence, we cannot determine the second-order rate constant, but we can nevertheless estimate the rate constant, using the initial rate of H_2O_2 consumption.

In Fig. 3 the normalized H_2O_2 concentration is plotted versus reaction time. As can be seen in the figure, H_2O_2 is in excess in all the experiments, i.e., is not completely consumed at the end of the experiment (when all UO_2 is consumed).

Previous studies, performed on micrometer-sized (~8 μm) UO_2 particles, have shown that approximately 80% of the total amount of consumed H_2O_2 leads to oxidation of UO_2 [19], this could however change when reducing the particle size to nanometer-scale. The magnitude of the catalytically decomposed H_2O_2 fraction is given by the ratio between the rate constants of the two competing reactions (oxidation of UO_2 and catalytic decomposition). The pre-

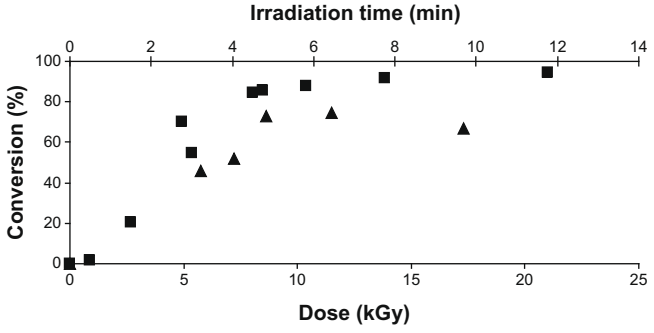

Fig. 1. Conversion of U(VI) as a function of irradiation time and absorbed dose, electron-irradiation (■) 2-PrOH system, (▲) *t*-BuOH system.

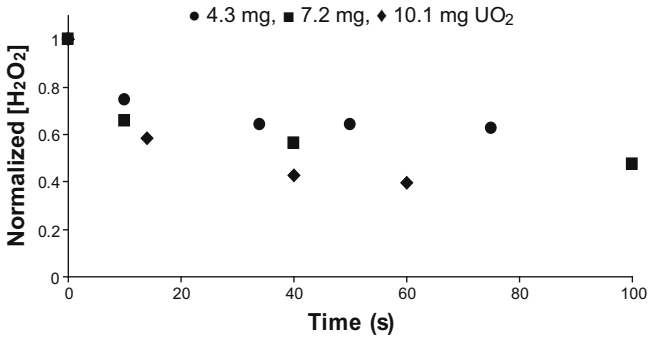

Fig. 3. Normalized concentration of H_2O_2 as a function of reaction time, for different amounts of added UO_2 powder.

exponential factor should be equal for the two reactions regardless of the particle size (assuming similar surface structure), since it is determined by the rate of diffusion in the system. If the particle size effect on the activation energy follows Eq. (5), the difference in activation energy between the two reactions should also remain constant when going from bulk material to nanoparticles. However, Eq. (5) was only derived for redox reactions and there are indications that the activation energy for catalytic decomposition is insensitive to changes in particle size and the type of metal-oxide [44]. In this case, assuming that Eq. (5) is valid for the oxidation of UO_2, the activation energy for oxidation of the nanometer-sized (~30 nm) material is calculated to be 10.6 kJ/mol higher than the activation energy for the catalytic decomposition.

The difference in activation energy can also be estimated based on the measured *G*-value for uranyl and the measured H_2O_2 consumption. From this data the catalytically decomposed H_2O_2 fraction is estimated to ~80%, corresponding to a difference in activation energy of around 7 kJ/mol. Considering the fairly large uncertainties into account this agrees relatively well with the activation energy difference calculated above.

The mechanism for oxidation of UO_2 by H_2O_2 is described by the following reactions.

$$H_2O_2 + UO_2(s) \rightarrow OH^{\bullet} + OH^- + UO_2^+(s) \quad (8)$$

$$OH^{\bullet} + UO_2^+(s) \rightarrow OH^+ + UO_2^{2+}(s) \quad (9)$$

It has previously been shown that the rate limiting step for this reaction is the first one-electron transfer reaction (8) [17], and the rate constant, using UO_2 powder of considerably larger size (~8 μm) than used in the present study, has been determined to 7.3×10^{-8} m/s [18]. The initial reaction rate for the nanometer-sized UO_2 is obtained from the initial slope in Fig. 3. By dividing the initial reaction rate by the initial H_2O_2 concentration and UO_2 surface area to solution volume ratio, a minimum value of the second-order rate constant can be estimated. The estimated rate constant is $\sim 2.5 \times 10^{-5}$ m/s ($\pm 1.0 \times 10^{-5}$), i.e., significantly higher than for the micrometer-sized powder.

Mennecart et al. and Grambow et al. have studied the dissolution and corrosion behavior of α-irradiated [25,26] and α-doped [24] UO_2 colloids of 3 nm size. The α-irradiated experiments indicated that the dissolution/corrosion behavior of the nanoparticles was similar to that of bulk UO_2. For the α-doped material the results were more difficult to interpret, but the authors claim that their results are in the range of previous results obtained for UO_2 pellets [45] and discs [46]. It should, however, be stressed, that the dissolution rate is not identical to the rate of oxidation unless steady-state is reached. Studies of the effect of HCO_3^- on the kinetics of UO_2 oxidation by H_2O_2 have shown that below 1 mM HCO_3^- both the oxidation and the dissolution governs the reaction, whereas for higher HCO_3^- concentrations the reaction is completely governed by oxidation [18]. Since the studies of UO_2 colloids by Mennecart et al. [25,26] and Grambow et al. [24] were all performed in the absence of HCO_3^-, the true rate constant for oxidation cannot be extracted from these data and hence, not compared to the results of the present work.

According to the relationship between the particle size and the activation energy given by Eq. (5), a decrease in particle size from 8 μm to 30 nm would lead to an increase in activation energy by 14 kJ/mol and, according to Eq. (4), the pre-exponential factor would increase by a factor of 267. As mentioned earlier, theoretically these effects are expected to cancel each other, and no change in the rate constant is expected.

In this study we have found that decreasing the particle size from micrometer range to nanometer range gives an increase in rate constant by a factor of ~340, i.e., very close to the theoretical increase in pre-exponential factor. This indicates that there is no significant particle size effect on the activation energy, this might seem surprising considering the expected quantum mechanical effects discussed in the introduction and the findings in Ref. [31].

However, since a large fraction of the H_2O_2 is catalytically decomposed (~80%) and the activation energy for this reaction is expected to be independent of particle size, the particle size dependence of the oxidation reaction will probably be of minor importance for the overall reactivity. In addition, due to the different methods of powder production, the surface structure of the materials (micrometer- and nanometer-sized powders) are not expected to be identical and hence, the rate constants obtained for the two powder types are not directly comparable. Furthermore, the relationship between the particle size and the reaction rate Eq. (4) is only valid for perfectly spherical particles. Since we do not have the possibility to synthesize completely spherical and monodisperse particles, it is impossible to accurately quantify the particle size effect on the pre-exponential factor in a real system.

It is nevertheless clear, that the radiolytically produced UO_2 nanoparticles are highly reactive when it comes to H_2O_2 consumption (significantly more reactive than the bulk powder). If such nanoparticles were produced and distributed in a deep repository for spent nuclear fuel, they could efficiently scavenge oxidants from the system and prevent further dissolution of the fuel matrix.

4. Conclusions

In this work we have studied the production of UO_2 nanoparticles by irradiating U(VI) solutions with electrons and γ-radiation. Electron-irradiation (high dose rate) in the presence of 2-propanol seems to be the most efficient method, showing high conversion of U(VI) and yielding small particles with a narrow size distribution (22–35 nm). At low pH and ionic strength the colloidal suspensions were stable over time. The results indicate that the powder does not consist of stoichiometric UO_2, but rather of a mixture of oxidation states; U(IV), U(V) and U(VI).

Furthermore, the reactivity of the produced nanoparticles towards H_2O_2 in the presence of HCO_3^- has been studied. The rate constant for this reaction was found to be significantly higher than for micrometer-sized UO_2. The increase in reactivity was close to the expected increase in pre-exponential factor, which is in good agreement with the large fraction of H_2O_2 being decomposed catalytically.

We have also shown that a similar material can be produced by the reduction of U(VI) by the solvated electron. This is a process that might be of importance in a future deep repository for spent nuclear fuel, were UO_2 nanoparticles could act as oxidant scavengers and hence inhibit the dissolution of the spent fuel matrix.

Acknowledgement

The Swedish Nuclear Fuel and Waste Management Co. is gratefully acknowledged for financial support.

References

[1] D.W. Shoesmith, J. Nucl. Mater. 282 (2000) 1. and references therein.
[2] O. Roth, M. Jonsson, Cent. Eur. J. Chem. 6 (2008) 1. and references therein.
[3] R.L. Segall, R.St.C. Smart, P.S. Turner, in: J. Nowotny, L.-C. Dufour (Eds.), Surface and Near-Surface Chemistry of Oxide Materials, Elsevier Science Publishers BV, Amsterdam, 1988, p. 527.
[4] M. Jonsson, F. Nielsen, O. Roth, E. Ekeroth, S. Nilsson, M.M. Hossain, Environ. Sci. Technol. 41 (2007) 7087.
[5] I. Grenthe, D. Ferri, F. Salvatore, G. Riccio, J. Chem. Soc., Dalton Trans. 11 (1984) 2439.
[6] D. Hayes, O.I. Mićić, M.T. Nenadović, V. Swayambunathan, D. Meisel, J. Phys. Chem. 93 (1989) 4603.
[7] M. Mostafavi, Y. Liu, P. Pernot, J. Belloni, Radiat. Phys. Chem. 59 (2000) 49.

[8] A.H. Souici, N. Keghouche, J.A. Delaire, H. Remita, M. Mostafavi, Chem. Phys. Lett. 422 (2006) 25.
[9] C. Lume-Pereira, S. Baral, A. Henglein, E. Janata, J. Phys. Chem. 89 (1985) 5772.
[10] J. Belloni, Catal. Today 113 (2006) 141. and references therein.
[11] J. Dzięgielewski, J. Kaleciński, B. Jeżowska-Trzebiatowska, Bull. Acad. Pol. Sci.-Chim. 12 (1964) 537.
[12] J. Dzięgielewski, J. Kaleciński, B. Jeżowska-Trzebiatowska, Bull. Acad. Pol. Sci.-Chim. 12 (1964) 545.
[13] J. Dzięgielewski, J. Kaleciński, Bull. Acad. Pol. Sci.-Chim. 17 (1969) 233.
[14] J. Dzięgielewski, B. Jeżowska-Trzebiatowska, J. Kaleciński, Bull. Acad. Pol. Sci.-Chim. 17 (1969) 239.
[15] E. Ekeroth, M. Jonsson, T.E. Eriksen, K. Ljungqvist, S. Kovács, I. Puigdomenech, J. Nucl. Mater. 334 (2004) 35.
[16] M.D. Kaminski, N.M. Dimitrijevic, C.J. Mertz, M.M. Goldberg, J. Nucl. Mater. 347 (2005) 77.
[17] E. Ekeroth, M. Jonsson, J. Nucl. Mater. 322 (2003) 242.
[18] M.M. Hossain, E. Ekeroth, M. Jonsson, J. Nucl. Mater. 358 (2006) 202.
[19] M. Jonsson, E. Ekeroth, O. Roth, Mat. Res. Soc. Symp. Proc. 807 (2004) 77.
[20] J. Merino, E. Cera, J. Bruno, J. Quiñones, I. Casas, F. Clarens, J. Giménez, J. De Pablo, M. Rovira, A. Martínez-Esparza, J. Nucl. Mater. 346 (2005) 40.
[21] J. de Pablo, I. Casas, J. Giménez, M. Molera, M. Rovira, L. Duro, J. Bruno, Geochim. Cosmochim. Acta 63 (1999) 3097.
[22] J. Belloni, M. Mostafavi, J.L. Marignier, J. Ambiard, J. Imaging Sci. 35 (1992) 68.
[23] T.P. Salikhov, V.V. Kan, Int. J. Thermophys. 26 (2005) 1215.
[24] T. Mennecart, B. Grambow, M. Fattahi, Z. Andriambololona, Radiochim. Acta 92 (2004) 611.
[25] T. Mennecart, B. Grambow, M. Fattahi, G. Blondiaux, Z. Andriambololona, Mat. Res. Soc. Symp. Proc. 807 (2004) 403.
[26] B. Grambow, T. Mennecart, M. Fattahi, G. Blondiaux, Radiochim. Acta 92 (2004) 603.
[27] U. Colombo, G. Fagherazzi, F. Gazzarrini, G. Lanzavecchia, G. Sironi, Nature 219 (1968) 1036.
[28] K.J. Gallagher, W. Feitknecht, U. Mannweiler, Nature 217 (1968) 1118.
[29] R.D. Astumian, Z.A. Shelly, J. Am. Chem. Soc. 106 (1984) 304.
[30] M.A. Nejad, M. Jonsson, J. Nucl. Mater. 334 (2004) 28.
[31] O. Roth, T. Bönnemark, M. Jonsson, J. Nucl. Mater. 353 (2006) 75.
[32] J. Belloni, M. Mostafavi, H. Remita, J.L. Marignier, M.O. Delcourt, New J. Chem. 22 (1998) 1239.
[33] M.O. Delcourt, J. Belloni, Radiochem. Radioanal. Lett. 13 (1973) 329.
[34] M. Haissinsky, in: J. Dobo, P. Hedvig (Eds.), Radiation Chemistry, vol. II, Akad. Kiado, Budapest, 1972, p. 1353.
[35] A. Henglein Progr, Colloid Polym. Sci. 73 (1987) 1.
[36] J.T. Nurmi, P.G. Tratnyek, V. Sarathy, D.R. Baer, J.E. Amonette, K. Pecher, C. Wang, J.C. Linehan, D.W. Matson, R.L. Penn, M.D. Driessen, Environ. Sci. Technol. 39 (2005) 1221.
[37] I.K. Kressin, Anal. Chem. 56 (1984) 2269.
[38] S.B. Savvin, Talanta 8 (1961) 673.
[39] W.A. Patrick, H.B. Wagner, Anal. Chem. 21 (1949) 1279.
[40] T.C.J. Ovenston, W.T. Rees, Analyst 75 (1950) 204.
[41] Y. Nimura, K. Itagaki, K. Nanba, Nippon Suisan Gakk. 58 (1992) 1129.
[42] M. Olsson, A.-M. Jakobsson, Y. Albinsson, J. Colloid Interface Sci. 256 (2002) 256.
[43] J.W.T. Spinks, R.J. Woods, An Introduction to Radiation Chemistry, 3rd Ed., John Wiley & Sons, Inc., New York, 1990.
[44] A. Hiroki, J.A. LaVerne, J. Phys. Chem. 109 (2005) 3364.
[45] C. Jégou, V. Broudic, A. Poulesquen, J.M. Bart, Mat. Res. Soc. Symp. Proc. 807 (2004) 391.
[46] S. Stroes-Gascoyne, F. King, J.S. Betteridge, F. Garisto, Radiochim. Acta 90 (2002) 603.